Generalized rate-code model for neuron ensembles with finite populations

Hideo Hasegawa*
Department of Physics, Tokyo Gakugei University, Koganei, Tokyo 184-8501, Japan
(Received 16 August 2006; revised manuscript received 13 December 2006; published 8 May 2007)

We have proposed a generalized Langevin-type rate-code model subjected to multiplicative noise, in order to study stationary and dynamical properties of an ensemble containing a finite number N of neurons. Calculations using the Fokker-Planck equation have shown that, owing to the multiplicative noise, our rate model yields various kinds of stationary non-Gaussian distributions such as Γ, inverse-Gaussian-like, and log-normal-like distributions, which have been experimentally observed. The dynamical properties of the rate model have been studied with the use of the augmented moment method (AMM), which was previously proposed by the author from a macroscopic point of view for finite-unit stochastic systems. In the AMM, the original N-dimensional stochastic differential equations (DEs) are transformed into three-dimensional deterministic DEs for the means and fluctuations of local and global variables. The dynamical responses of the neuron ensemble to pulse and sinusoidal inputs calculated by the AMM are in good agreement with those obtained by direct simulation. The synchronization in the neuronal ensemble is discussed. The variabilities of the firing rate and of the interspike interval are shown to increase with increasing magnitude of multiplicative noise, which may be a conceivable origin of the observed large variability in cortical neurons.

DOI: 10.1103/PhysRevE.75.051904 PACS number(s): 87.10.+e, 84.35.+i

I. INTRODUCTION

Neurons in a brain communicate information, emitting spikes which propagate through axons and dendrites to neurons at the next stage. It has been a long-standing controversy whether the information in neurons is encoded in the firing rates (rate code) or in the more precise firing times (temporal code) [1–3]. Some experimental results that have been reported seem to support the former code while some the latter [1–3]. In particular, a recent success in a brain-machine interface [4,5] suggests that the population rate code is employed in sensory and motor neurons while it is still not clear which code is adopted in higher-level cortical neurons.

Experimental observations have shown that, in many areas of the brain, neurons are organized into groups of cells such as columns in the visual cortex [6]. A small patch in the cortex contains thousands of similar neurons, which receive inputs from the same patch and other patches. There are many theoretical studies of the property of neuronal ensembles consisting of equivalent neurons, with the use of spiking neuron models or rate-code models (for a review of neuronal models, see [7], and related references therein). In the spiking neuron model, the dynamics of the membrane potential of a neuron in the ensemble is described by the Hodgkin-Huxley- (HH-) type nonlinear differential equations (DEs) [8] which express the conductance-based mechanism for firings. Reduced, simplified models such as the integrate-and-fire (IF) and FitzHugh-Nagumo (FN) models have also been employed. In contrast, in the rate-code model, neurons are regarded as transducers between input and output signals, both of which are expressed in terms of spiking rates.

Computational neuroscientists have tried to understand the properties of ensemble neurons by using the two approaches: direct simulations (DSs) and analytical approaches. DS calculations have been performed for large-scale networks mostly described by the simplest IF model. Since the computational time of DS grows as N^2 with N, the size of the ensemble, a large-scale DS with more realistic models becomes difficult. Although DS calculations provide us with useful insight into the firing activity of the ensemble, it is desirable to have results obtained by using analytical approaches.

Analytical or semianalytical calculation methods for neuronal ensembles have been proposed by using the mean-field (MF) method [9–11], population-density approaches [12–16], the moment method [17], and the augmented moment method (AMM) [18] (details of the AMM will be discussed shortly). It is interesting to analytically obtain information about the firing rate or the interspike interval (ISI), starting from the spiking neuron model. It has been shown that the dynamics of the spiking neuron ensemble may be described by DEs of a macroscopic variable for the population density or spike activity, which determines the firing rate of ensemble neurons [12–16]. By using the f-I relation between the applied dc current I and the frequency f of autonomous firings, the rate-code model for conduction-based neuron models is derived [19–21]. When we apply the Fokker-Planck equation (FPE) method to the neuron ensemble described by the IF model, the averaged firing rate $R(t)$ is expressed by $P(V,\theta,t)$, which denotes the distribution probability of the averaged membrane potential V with the threshold θ for the firing [22].

It is well known that neurons in brains are subjected to various kinds of noise, although its precise origins are not well understood. The response of neurons to stimuli is expected to be modified by noise in various ways. Indeed, although firings of a single *in vitro* neuron are reported to be precise and reliable [23], those of *in vivo* neurons are quite unreliable due to the noisy environment. The strong criticism against the temporal code is that it is not robust against noise, while the rate code is robust.

*Electronic address: hasegawa@u-gakugei.ac.jp

It is commonly assumed that there are two types of noise: additive and multiplicative noise. The magnitude of the former is independent of the state of the variable while that of the latter depends on its state. Interesting phenomena caused by the two types of noise have been investigated [24]. It has been found that the property of multiplicative noise is different from that of additive noise in some respects. (1) Multiplicative noise induces a phase transition, creating an ordered state, while additive noise works to destroy the ordering [25,26]. (2) Although the probability distribution in stochastic systems subjected to additive white noise follows a Gaussian, multiplicative white noise generally yields a non-Gaussian distribution [27–32]. (3) The scaling relation of the effective strength for additive noise given by $\beta(N)=\beta(1)/\sqrt{N}$ is not applicable to that for multiplicative noise: $\alpha(N)\neq\alpha(1)/\sqrt{N}$, where $\alpha(N)$ and $\beta(N)$ denote the effective strengths of multiplicative and additive noise, respectively, in the N-unit system [33]. A naive approximation of the scaling relation for multiplicative noise, $\alpha(N)=\alpha(1)/\sqrt{N}$ as adopted in Ref. [25], yields a result that does not agree with that of DS [33].

In this paper, we will study the properties of neuronal ensembles based on the rate-code hypothesis. The rate models that have been proposed so far are mainly given by [4]

$$\frac{dr_i(t)}{dt}=-\lambda r_i(t)+H\left(\frac{1}{N}\sum_j w_{ij}r_j(t)+I_i(t)\right)+\beta\xi_i(t), \quad (1)$$

where $r_i(t)$ $(\geqslant 0)$ denotes the firing rate of a neuron i $(i=1-N)$, λ the relaxation rate, w_{ij} the coupling strength, $H(x)$ the gain function, $I_i(t)$ an external input, and β the magnitude of additive white noise of $\xi_i(t)$ with the correlation $\langle\xi_i(t)\xi_j(t')\rangle=\delta_{ij}\delta(t-t')$. The rate model as given by Eq. (1) has been adopted in many models based on neuronal population dynamics. The typical rate model is the Wilson-Cowan model, with which the stability of an ensemble consisting of excitatory and inhibitory neurons is investigated [12,34]. The rate model given by Eq. (1) with $H(x)=x$ is the Hopfield model [35], which has been extensively adopted for studies of the memory in the brain incorporating the plasticity of synapses into w_{ij}. DS calculations have been performed, for example, for a study of the population coding for $N=100$ [4]. Analytical studies of Eq. (1) are conventionally made for the case of $N=\infty$, adopting the FPE method with MF and diffusion approximations. The stationary distribution obtained by the FPE for Eq. (1) generally follows the Gaussian distribution.

ISI data obtained from experiments have been fitted by a superposition of some known probability densities such as the Γ, inverse-Gaussian, and log-normal distributions [36–40]. The Γ distribution with parameters λ and μ is given by

$$P_{gam}(x)=\frac{\mu^{-\lambda}}{\Gamma(\lambda)}x^{\lambda-1}\exp\left(-\frac{x}{\mu}\right), \quad (2)$$

which is derived from a simple stochastic IF model with additive noise for Poisson inputs [37], $\Gamma(x)$ being the gamma function. For $\lambda=1$ in Eq. (2), we get the exponential distribution describing a standard Poisson process. The inverse Gaussian distribution with parameters λ and μ given by

$$P_{IG}(x)=\left(\frac{\lambda}{2\pi x^3}\right)^{1/2}\exp\left(-\frac{\lambda(x-\mu)^2}{2\mu^2 x}\right), \quad (3)$$

and is obtained from a stochastic IF model in which the membrane potential is represented as a random walk with drift [36]. The log-normal distribution with parameters μ and σ given by

$$P_{LN}(x)=\frac{1}{\sqrt{2\pi\sigma^2 x}}\exp\left(-\frac{(\ln x-\mu)^2}{2\sigma^2}\right), \quad (4)$$

is adopted when the logarithm of ISI is assumed to follow a Gaussian form [38]. Fittings of experimental ISI data to a superposition of these probability densities have been extensively discussed in the literature [36–40].

The purpose of the present paper is to propose and study the generalized, phenomenological rate model [Eqs. (5) and (6)]. We will discuss ensembles with finite populations, contrary to most existing analytical theories except a few (e.g., Ref. [16]), which discuss ensembles with infinite N. The stationary distribution of our rate model will be discussed by using the FPE method. It is shown that, owing to the introduced multiplicative noise, our rate model yields not only the Gaussian distribution but also non-Gaussian distributions such as Γ, inverse-Gaussian-like, and log-normal-like distributions.

The dynamical properties of our rate model will be studied by using the AMM, which was previously proposed by the present author [18,33,41]. Based on a macroscopic point of view, Hasegawa [18] proposed the AMM, which emphasizes not the properties of individual neurons but rather those of ensemble neurons. In the AMM, the state of finite-N-unit stochastic ensembles is described by a fairly small number of variables: averages and fluctuations of local and global variables. For example, the number of deterministic equations in the AMM becomes 3 for an N-unit Langevin model. The AMM has been successfully applied to a study on the dynamics of the Langevin model and stochastic spiking neuron models such as FN and HH models, with global, local, or small-world couplings (with and without transmission delays) [42–46].

The AMM in [18] was originally developed by expanding variables around their stable mean values in order to obtain the second-order moments for both local and global variables in stochastic systems. In recent papers [33,41], we have reformulated the AMM with the use of the FPE to discuss stochastic systems subjected to multiplicative noise: the FPE is adopted to avoid the difficulty due to the Ito versus Stratonovich calculus inherent to multiplicative noise. In the present paper, a study on the Langevin model with multiplicative noise made in [41], has been applied to an investigation on the firing properties of neuronal ensembles. Our method aims at the same purpose to effectively study the property of neuronal ensembles as the approaches developed in Refs. [12–16,19–21].

The paper is organized as follows. In Sec. II, we discuss the generalized rate model for an ensemble containing N neurons, investigating its stationary and dynamical properties. Some discussions are presented in Sec. III, where variabilities of the rate and ISI are calculated. The final Sec. IV is devoted to our conclusion.

II. PROPERTY OF NEURON ENSEMBLES

A. Generalized rate-code model

For a study of the properties of a neuron ensemble containing a finite number N of neurons, we have assumed that the dynamics of the firing rate $r_i(t)$ (≥ 0) of a neuron i ($i=1-N$) is given by

$$\frac{dr_i}{dt} = F(r_i) + H(u_i) + \alpha G(r_i)\eta_i(t) + \beta\xi_i(t), \tag{5}$$

with

$$u_i(t) = \left(\frac{w}{Z}\right)\sum_{j(\neq i)} r_j(t) + I_i(t). \tag{6}$$

Here $F(x)$, $G(x)$, and $H(x)$ are arbitrary functions of x, Z ($=N-1$) denotes the coordination number, $I_i(t)$ is an input from external sources, and w is the coupling strength; α and β express the strengths of additive and multiplicative noise, respectively, given by $\xi_i(t)$ and $\eta_i(t)$, which express zero-mean Gaussian white noise with correlations given by

$$\langle \eta_i(t)\eta_j(t')\rangle = \delta_{ij}\delta(t-t'), \tag{7}$$

$$\langle \xi_i(t)\xi_j(t')\rangle = \delta_{ij}\delta(t-t'), \tag{8}$$

$$\langle \eta_i(t)\xi_j(t')\rangle = 0. \tag{9}$$

The rate model in Eq. (1) adopts $F(x)=-\lambda x$ and $G(x)=0$ (no multiplicative noise).

The gain function $H(x)$ expresses the response of the firing rate (r_i) to a synaptic input field (u_i). It has been theoretically shown in [47] that, when spike inputs with the mean ISI (T_{in}) are applied to an HH neuron, the mean ISI of output signals (T_{out}) is $T_{out}=T_{in}$ for $T_{in}\gtrsim 15$ ms and $T_{out}\sim 15$ ms for $T_{in}\lesssim 15$ ms. This is consistent with the recent calculation for HH neuron multilayers [48], which shows a nearly linear relationship between the input (r_{in}) and output rates (r_{out}) for $r_{in}<60$ Hz (Fig. 3 of Ref. [48]). It is interesting that the r_{in}-r_{out} relation is continuous despite the fact that the f-I relation of the HH neuron shows a discontinuous, type-II behavior according to Ref. [8]. In the literature, two types of expressions for $H(x)$ have been adopted so far. In the first category, sigmoid functions such as $H(x)=1/(1+e^{-x})$ (e.g., [12]) and arctan(x) (e.g., [49]) have been adopted. In the second category, gain functions such as $H(x)=(x-x_c)\Theta(x-x_c)$ (e.g., [21]) have been employed, modeling the f-I function for the frequency f of autonomous oscillation against the applied dc current I, x_c expressing the critical value and $\Theta(x)$ the Heaviside function: $\Theta(x)=1$ for $x\geq 0$ and 0 otherwise. The nonlinear, saturating behavior in $H(x)$ arises from the property of the refractory period (τ_r) because spike outputs are prevented for $t_f<t<t_f+\tau_r$ after firing at $t=t_f$. In this paper, we have adopted a simple expression given by [50]

$$H(x) = \frac{x}{\sqrt{x^2+1}}, \tag{10}$$

although our results to be presented in the following sections are expected to be valid for any choice of $H(x)$.

B. Stationary properties

1. Distribution of r

By employing the FPE, we may discuss the stationary distribution $p(r)$ for $w=0$ and $I_i(t)=I$, which is given by [30,31]

$$\ln p(r) \propto X(r) + Y(r) - \left(1-\frac{\phi}{2}\right)\ln\left(\frac{\alpha^2 G(r)^2}{2}+\frac{\beta^2}{2}\right), \tag{11}$$

with

$$X(r) = 2\int dr\left(\frac{F(r)}{\alpha^2 G(r)^2+\beta^2}\right), \tag{12}$$

$$Y(r) = 2\int dr\left(\frac{H(I)}{\alpha^2 G(r)^2+\beta^2}\right), \tag{13}$$

where $\phi=0$ and 1 for the Ito and Stratonovich representations, respectively. Hereafter we mainly adopt the Stratonovich representation.

Case I. $F(x)=-\lambda x$ and $G(x)=x$. For the linear Langevin model, we get

$$p(r) \propto \left[1+\left(\frac{\alpha^2 r^2}{\beta^2}\right)\right]^{-(\lambda/\alpha^2+1/2)} e^{Y(r)}, \tag{14}$$

with

$$Y(r) = \left(\frac{2H}{\alpha\beta}\right)\arctan\left(\frac{\alpha r}{\beta}\right), \tag{15}$$

where $H=H(I)$. In the case of $H=Y(r)=0$, we get the q-Gaussian given by [30,31]

$$p(r) \propto [1-(1-q)\gamma r^2]^{1/(1-q)}, \tag{16}$$

with

$$\gamma = \frac{2\lambda+\alpha^2}{2\beta^2}, \tag{17}$$

$$q = \frac{2\lambda+3\alpha^2}{2\lambda+\alpha^2}. \tag{18}$$

We examine some limiting cases of Eq. (14) as follows.

(a) For $\alpha=0$ and $\beta\neq 0$ (i.e., additive noise only), Eq. (14) yields

$$p(r) \propto e^{-(\lambda/\beta^2)(r-H/\lambda)^2}. \tag{19}$$

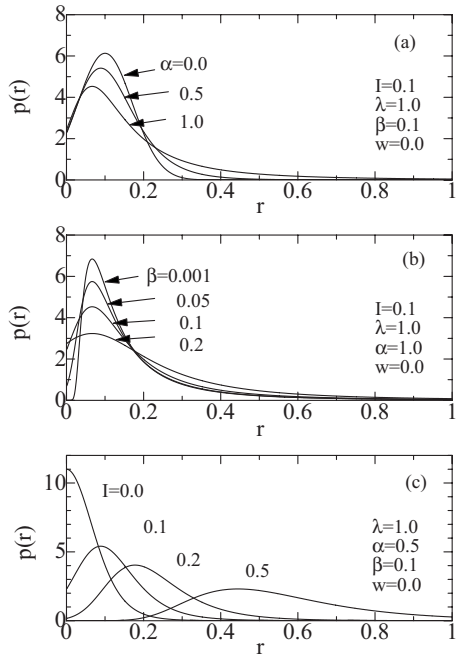

FIG. 1. (a) Distributions $p(r)$ of the (local) firing rate r for various α with $\lambda=1.0$, $\beta=0.1$, $I=0.1$, and $w=0.0$, (b) $p(r)$ for various β with $\lambda=1.0$, $\alpha=1.0$, $I=0.1$, and $w=0.0$, and (c) $p(r)$ for various I with $\lambda=1.0$, $\alpha=0.5$, $\beta=0.1$, and $w=0.0$.

(b) For $\beta=0$ and $\alpha\neq 0$ (i.e., multiplicative noise only), Eq. (14) leads to

$$p(r) \propto r^{-(2\lambda/\alpha^2+1)} e^{-(2H/\alpha^2)/r}. \tag{20}$$

Distributions $p(r)$ calculated with the use of Eqs. (14)–(20) are plotted in Figs. 1(a)–1(c). The distribution $p(r)$ for $\alpha=0.0$ (without multiplicative noise) in Fig. 1(a) shows the Gaussian distribution, which is shifted by an applied input $I=0.1$. When multiplicative noise is added ($\alpha\neq 0$), the form of $p(r)$ is changed to the q-Gaussian given by Eq. (16). Figure 1(b) shows that, when the magnitude of additive noise β is increased, the width of $p(r)$ is increased. Figure 1(c) shows that, when the magnitude of the external input I is increased, $p(r)$ is much shifted and widely spread. Note that, for $\alpha=0.0$ and $\beta\neq 0$ (additive noise only), $p(r)$ is simply shifted without a change in its shape when increasing I [Eq. (19)].

Case II. $F(x)=-\lambda x^a$ *and* $G(x)=x^b$ $(a,b\geqslant 0)$. The special case of $a=1$ and $b=1$ has been discussed in the preceding case I [Eqs. (14)–(20)]. For arbitrary a $(\geqslant 0)$ and b $(\geqslant 0)$, the probability distribution $p(r)$ given by Eqs. (11)–(13) becomes

$$p(r) \propto \left[1+\left(\frac{\alpha^2}{\beta^2}\right)r^{2b}\right]^{-1/2} e^{X(r)+Y(r)}, \tag{21}$$

with

$$X(r) = -\left(\frac{2\lambda r^{a+1}}{\beta^2(a+1)}\right) F\left(1, \frac{a+1}{2b}, \frac{a+1}{2b}+1; -\frac{\alpha^2 r^{2b}}{\beta^2}\right), \tag{22}$$

$$Y(r) = \left(\frac{2Hr}{\beta^2}\right) F\left(1, \frac{1}{2b}, \frac{1}{2b}+1; -\frac{\alpha^2 r^{2b}}{\beta^2}\right), \tag{23}$$

where $F(a,b,c;z)$ is the hypergeometric function. Some limiting cases of Eqs. (21)–(23) are shown in the following.

(a) The case of $H=Y(r)=0$ was previously studied in [31].

(b) For $\alpha=0$ and $\beta\neq 0$ (i.e., additive noise only), we get

$$p(r) \propto \exp\left[-\left(\frac{2\lambda}{\beta^2(a+1)}\right)r^{a+1} + \left(\frac{2H}{\beta^2}\right)r\right]. \tag{24}$$

(c) For $\beta=0$ and $\alpha\neq 0$ (i.e., multiplicative noise only), we get

$$p(r) \propto \begin{cases} r^{-b}\exp\left[-\left(\dfrac{2\lambda}{\alpha^2(a-2b+1)}\right)r^{a-2b+1} - \left(\dfrac{2H}{\alpha^2(2b-1)}\right)r^{-2b+1}\right] & \text{for } a-2b+1\neq 0, 2b-1\neq 0, \quad (25) \\ r^{-(2\lambda/\alpha^2+b)}\exp\left[-\left(\dfrac{2H}{\alpha^2(2b-1)}\right)r^{-2b+1}\right] & \text{for } a-2b+1=0 \quad (26) \\ r^{(2H/\alpha^2-1/2)}\exp\left[-\left(\dfrac{2\lambda}{\alpha^2 a}\right)r^a\right] & \text{for } 2b-1=0 \quad (27) \\ r^{-[2(\lambda-H)/\alpha^2+1/2]} & \text{for } a-2b+1=0, 2b-1=0 \quad (28) \end{cases}$$

(d) In the case of $a=1$ and $b=1/2$, we get

$$p(r) \propto \left(r+\frac{\beta^2}{\alpha^2}\right)^{(2\lambda\beta^2/\alpha^4+2H/\alpha^2-1/2)} \exp\left[-\left(\frac{2\lambda}{\alpha^2}\right)r\right], \tag{29}$$

which reduces, in the limit of $\alpha=0$, to

$$p(r) \propto \exp\left[-\left(\frac{\lambda}{\beta^2}\right)\left(r-\frac{H}{\lambda}\right)^2\right] \quad \text{for } \alpha=0. \tag{30}$$

Case III. $F(x)=-\lambda \ln x$ *and* $G(x)=x^{1/2}$. We get

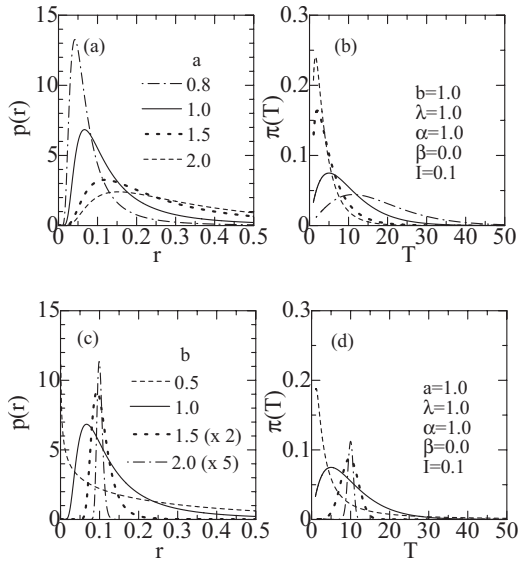

FIG. 2. (a) Distributions $p(r)$ of the (local) firing rate r and (b) $\pi(T)$ of the ISI T for $a=0.8$ (dot-dashed curves), 1.0 (solid curves), 1.5 (dotted curves), and 2.0 (dashed curves) with $\lambda=1.0$, $b=1.0$, $I=0.1$, $\alpha=1.0$, and $\beta=0.0$ (multiplicative noise only). (c) $p(r)$ of the (local) firing rate r and (d) $\pi(T)$ of the ISI T for $b=0.5$ (dashed curves), 1.0 (solid curves), 1.5 (dotted curves), and 2.0 (dot-dashed curves) with $\lambda=1.0$, $a=1.0$, $I=0.1$, $\alpha=1.0$, and $\beta=0.0$ (multiplicative noise only); results for $b=1.5$ and $b=2$ should be multiplied by factors of 2 and 5, respectively.

$$p(r) \propto r^{-1/2} \exp\left[-\left(\frac{\lambda}{\alpha^2}\right)\left(\ln r - \frac{H}{\lambda}\right)^2\right] \quad \text{for } \beta = 0. \tag{31}$$

Figure 2(a) shows distributions $p(r)$ for case II and various a with fixed values of $\lambda=1.0$, $b=1.0$, $I=0.1$, $\alpha=1.0$, and $\beta=0.0$ (multiplicative noise only). With further decrease in a, the peak of $p(r)$ at $r\sim 0.1$ becomes sharper. Figure 2(c) shows distributions $p(r)$ for case II and various b with fixed values of $\lambda=1.0$, $a=1.0$, $I=0.1$, $\alpha=1.0$, and $\beta=0.0$ (multiplicative noise only). We note that a change in the b value yields considerable changes in the shape of $p(r)$. Figures 2(b) and 2(d) will be discussed shortly.

2. Distribution of T

When the temporal ISI T is simply defined by $T=1/r$, its distribution $\pi(T)$ is given by

$$\pi(T) = p\left(\frac{1}{T}\right)\frac{1}{T^2}. \tag{32}$$

We get various distributions of $\pi(T)$ depending on the functional forms of $F(x)$ and $G(x)$. For $F(x)=-\lambda x$, $G(x)=x$, and $\beta=0$, Eq. (26) yields

$$\pi(T) \propto T^{(2\lambda/\alpha^2-1)} \exp\left[-\left(\frac{2H}{\alpha^2}\right)T\right], \tag{33}$$

which expresses the Γ distribution [Eq. (2)] [29,37]. For $F(x)=-\lambda x^2$, $G(x)=x$, and $\beta=0$, Eq. (25) leads to

$$\pi(T) \propto T^{-1} \exp\left[-\left(\frac{2H}{\alpha^2}\right)T - \left(\frac{2\lambda}{\alpha^2}\right)\frac{1}{T}\right], \tag{34}$$

which is similar to the inverse Gaussian distribution [Eq. (3)] [36]. For $F(x)=-\lambda \ln x$, $G(x)=x^{1/2}$, and $\beta=0$, Eq. (31) yields

$$\pi(T) \propto T^{-3/2} \exp\left[-\left(\frac{2\lambda}{\alpha^2}\right)\left(\ln T + \frac{H}{\lambda}\right)^2\right], \tag{35}$$

which is similar to the log-normal distribution [Eq. (4)] [38].

Figures 2(b) and 2(d) show $\pi(T)$ obtained from $p(r)$ shown in Figs. 2(a) and 2(c), respectively, by a change of variable with Eq. (32). Figure 2(b) shows that, with further decrease in a, the peak of $\pi(T)$ becomes sharper and moves left. We note in Fig. 2(d) that the form of $\pi(T)$ is significantly varied by changing b in $G(x)=x^b$.

3. Distribution of R

When we consider the global variable $R(t)$ defined by

$$R(t) = \frac{1}{N}\sum_i r_i(t), \tag{36}$$

the distribution $P(R,t)$ for R is given by

$$P(R,t) = \int \cdots \int \Pi_i dr_i p(\{r_i\},t)\,\delta\left(R - \frac{1}{N}\sum_j r_j\right). \tag{37}$$

Analytic expressions for $P(R)$ are obtainable only for limited cases.

(a) For $\beta\neq 0$ and $\alpha=0$, $P(R)$ is given by

$$P(R) \propto \exp\left[-\left(\frac{\lambda N}{\beta^2}\right)\left(R - \frac{H}{\lambda}\right)^2\right], \tag{38}$$

where $H=H(I)$.

(b) For $H=0$, we get [41]

$$P(R) = \frac{1}{2\pi}\int_{-\infty}^{\infty} dk\, e^{ikR}\Phi(k), \tag{39}$$

with

$$\Phi(k) = \left[\phi\left(\frac{k}{N}\right)\right]^N, \tag{40}$$

where $\phi(k)$ is the characteristic function for $p(r)$ given by [51]

$$\phi(k) = \int_{-\infty}^{\infty} e^{-ikr} p(r) dr, \tag{41}$$

$$= 2^{1-\nu}\frac{(\lambda'|k|)^\nu}{\Gamma(\nu)} K_\nu(\lambda'|k|), \tag{42}$$

with

$$\nu = \frac{\lambda}{\alpha^2}, \tag{43}$$

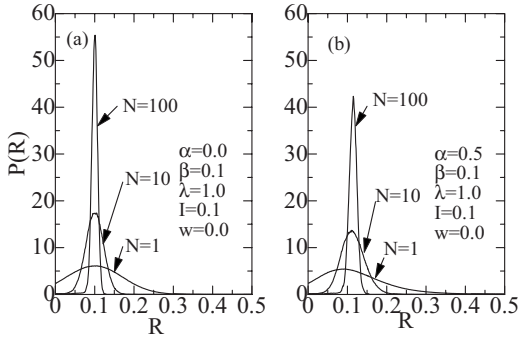

FIG. 3. Distributions $P(R)$ of the (global) firing rate R for α =(a) 0.0 and (b) 0.5, with N=1, 10, and 100; λ=1.0, β=0.1, w =0.0, and I=0.1.

$$\lambda' = \frac{\beta}{\alpha}, \tag{44}$$

$K_\nu(x)$ expressing the modified Bessel function.

Some numerical examples of $P(R)$ are plotted in Figs. 3–5. Figures 3(a) and 3(b) show $P(R)$ for α=0.0 and 0.5, respectively, when N is changed. For α=0.0, $P(R)$ is the Gaussian distribution whose width is narrowed by a factor of $1/\sqrt{N}$ with increasing N. In contrast, $P(R)$ for α=0.5 is non-Gaussian, whose shape seems to approach a Gaussian for increasing N. These are consistent with the central-limit theorem.

Effects of an external input I on $p(r)$ and $P(R)$ are examined in Figs. 4(a) and 4(b). Figure 4(a) shows that, in the case of α=0.0 (additive noise only), $p(r)$ and $P(R)$ are simply shifted by a change in I. This is not the case for $\alpha \neq 0.0$, for which $p(r)$ and $P(R)$ are shifted and widened with increasing I, as shown in Fig. 4(b).

Figures 5(a) and 5(b) show effects of the coupling w on $p(r)$ and $P(R)$. For α=0.0, $p(r)$ and $P(R)$ are changed only slightly with increasing w. On the contrary, for α=0.5, an introduction of the coupling significantly modifies $p(r)$ and $P(R)$ as shown in Fig. 5(b).

C. Dynamical properties

1. Augmented moment method

Next we will discuss the dynamical properties of the rate model by using the AMM [18,33,41]. By employing the

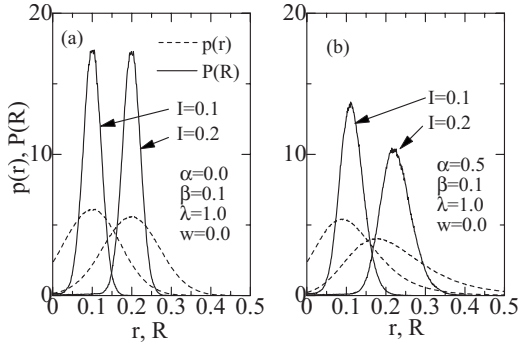

FIG. 4. Distributions $p(r)$ (dashed curves) and $P(R)$ (solid curves) for α=(a) 0.0 and (b) 0.5 with I=0.1 and 0.2; N=10, λ =1.0, β=0.1, and w=0.0.

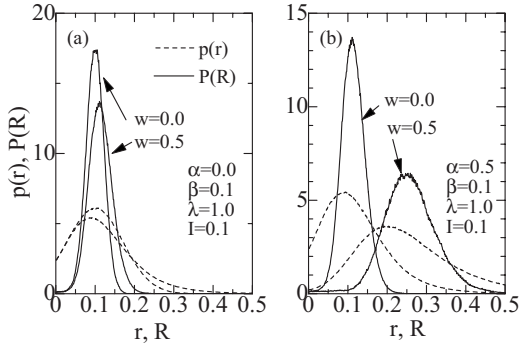

FIG. 5. Distributions $p(r)$ (dashed curves) and $P(R)$ (solid curves) for α=(a) 0.0 and (b) 0.5 with w=0.0 and 0.5; N=10, λ =1.0, β=0.1, and I=0.1.

FPE, we obtain the equations of motion for the moments $\langle r_i \rangle$, $\langle r_i r_j \rangle$, and $\langle R^2 \rangle$ where $R=(1/N)\Sigma_i r_i$. Then we get the equations of motion for the three quantities μ, γ, and ρ defined by [18,33,41]

$$\mu = \langle R \rangle = \frac{1}{N}\sum_i \langle r_i \rangle, \tag{45}$$

$$\gamma = \frac{1}{N}\sum_i \langle (r_i - \mu)^2 \rangle, \tag{46}$$

$$\rho = \langle (R - \mu)^2 \rangle, \tag{47}$$

where μ expresses the mean, γ the averaged fluctuations in local variables (r_i), and ρ the fluctuations in the global variable (R). We get (for details see [33,41])

$$\frac{d\mu}{dt} = f_0 + f_2\gamma + h_0 + \left(\frac{\phi\alpha^2}{2}\right)[g_0 g_1 + 3(g_1 g_2 + g_0 g_3)\gamma], \tag{48}$$

$$\frac{d\gamma}{dt} = 2f_1\gamma + 2h_1\left(\frac{wN}{Z}\right)\left(\rho - \frac{\gamma}{N}\right) + (\phi + 1)(g_1^2 + 2g_0 g_2)\alpha^2\gamma + \alpha^2 g_0^2 + \beta^2, \tag{49}$$

$$\frac{d\rho}{dt} = 2f_1\rho + 2h_1 w\rho + (\phi + 1)(g_1^2 + 2g_0 g_2)\alpha^2\rho + \frac{1}{N}(\alpha^2 g_0^2 + \beta^2), \tag{50}$$

where $f_\ell = (1/\ell!)[\partial^\ell F(\mu)/\partial x^\ell]$, $g_\ell = (1/\ell!)[\partial^\ell G(\mu)/\partial x^\ell]$, $h_\ell = (1/\ell!)[\partial^\ell H(u)/\partial u^\ell]$, and $u = w\mu + I$. The original N-dimensional stochastic DEs given by Eqs. (5) and (6) are transformed to the three-dimensional deterministic DEs given by Eqs. (48)–(50).

When we adopt

$$F(x) = -\lambda x, \tag{51}$$

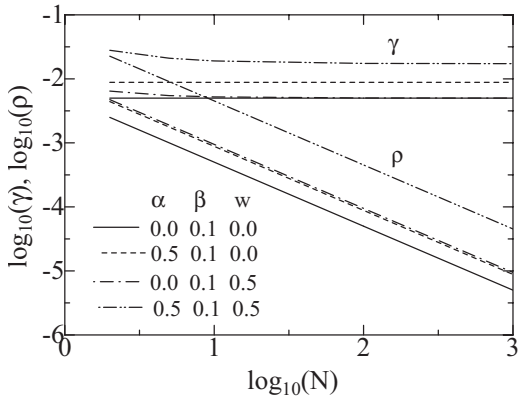

FIG. 6. N dependence of γ and ρ in the stationary states for four sets of parameters: $(\alpha,\beta,w)=(0.0,0.1,0.0)$ (solid curves), (0.5, 0.1, 0.0) (dashed curves), (0.0, 0.1, 0.5) (dot-dashed curves), and (0.5, 0.1, 0.5) (double-dot-dashed curves); $\lambda=1.0$, $N=10$, and $I=0.1$.

$$G(x) = x, \tag{52}$$

Eqs. (48)–(50) are expressed in the Stratonovich representation ($\phi=1$) by

$$\frac{d\mu}{dt} = -\lambda\mu + h_0 + \frac{\alpha^2\mu}{2}, \tag{53}$$

$$\frac{d\gamma}{dt} = -2\lambda\gamma + \frac{2h_1 wN}{Z}\left(\rho - \frac{\gamma}{N}\right) + 2\alpha^2\gamma + \alpha^2\mu^2 + \beta^2, \tag{54}$$

$$\frac{d\rho}{dt} = -2\lambda\rho + 2h_1 w\rho + 2\alpha^2\rho + \frac{\alpha^2\mu^2}{N} + \frac{\beta^2}{N}, \tag{55}$$

where $h_0=u/\sqrt{u^2+1}$, $h_1=1/(u^2+1)^{3/2}$, and $h_2=-(3u/2)/(u^2+1)^{5/2}$ with $u=w\mu+I$.

Before discussing the dynamical properties, we study the stationary properties of Eqs. (53)–(55). We get the stationary solution given by

$$\mu = \frac{h_0}{(\lambda - \alpha^2/2)}, \tag{56}$$

$$\gamma = \frac{(\alpha^2\mu^2 + \beta^2)}{2(\lambda - \alpha^2 + wh_1/Z)}\left(1 + \frac{wh_1}{Z(\lambda - \alpha^2 - wh_1)}\right), \tag{57}$$

$$\rho = \frac{(\alpha^2\mu^2 + \beta^2)}{2N(\lambda - \alpha^2 - wh_1)}, \tag{58}$$

where Eq. (56) expresses the fifth-order algebraic equation of μ. The stability of Eqs. (53)–(55) around the stationary solution may be shown by calculating eigenvalues of their Jacobian matrix, although the actual calculations are tedious.

Figure 6 shows the N dependences of γ and ρ in the stationary state for four sets of parameters: $(\alpha,\beta,w)=(0.0,0.1,0.0)$ (solid curves), (0.5, 0.1, 0.0) (dashed curves), (0.0, 0.1, 0.5) (dot-dashed curves), and (0.5, 0.1, 0.5) (double-dot-dashed curves), with $\beta=0.1$, $\lambda=1.0$, and $I=0.1$. For all the cases, ρ is proportional to N^{-1}, which is easily seen in Eq. (58). In contrast, γ shows a weak N dependence for small N (<10). It is noted that $\sqrt{\gamma}$ and $\sqrt{\rho}$ approximately express the widths of $p(r)$ and $P(R)$, respectively. The N dependence of ρ in Fig. 6 is consistent with the result shown in Figs. 3(a) and 3(b), and with the central-limit theorem.

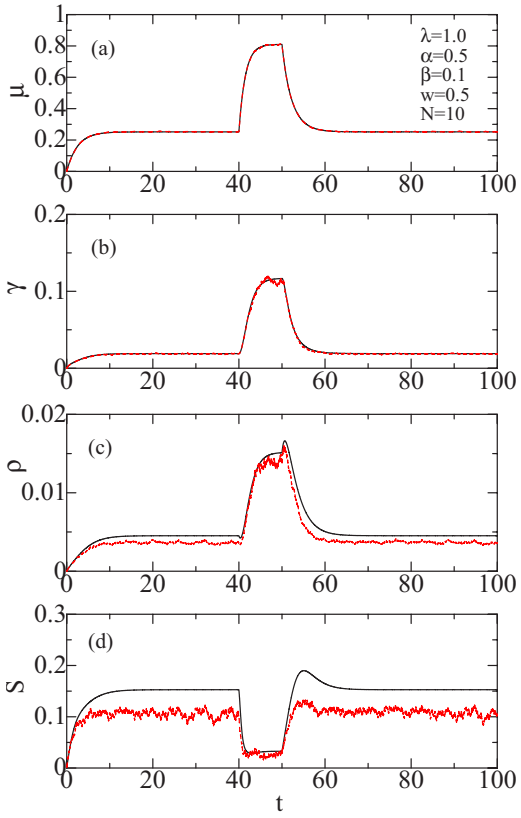

FIG. 7. (Color online) Time courses of (a) $\mu(t)$, (b) $\gamma(t)$, (c) $\rho(t)$, and (d) $S(t)$ for a pulse input $I(t)$ given by Eq. (59) with $\lambda=1.0$, $\alpha=0.5$, $\beta=0.1$, $N=10$, and $w=0.5$, solid and dashed curves denoting results of AMM and dashed curves expressing those of DS result with 1000 trials.

2. Response to pulse inputs

We have studied the dynamical properties of the rate model, by applying a pulse input of $I=I(t)$ given by

$$I(t) = A\Theta(t - t_1)\Theta(t_2 - t) + I^{(b)}, \tag{59}$$

with $A=0.5$, $t_1=40$, $t_2=50$, and $I^{(b)}=0.1$ which expresses the background input. Figures 7(a)–7(c) show the time dependences of μ, γ, and ρ for $F(x)=-\lambda x$ and $G(x)=x$ when the input pulse $I(t)$ given by Eq. (59) is applied [52]: solid and dashed curves show the results of the AMM and DS averaged over 1000 trials, respectively, with $\alpha=0.5$, $\beta=1.0$, $w=0.5$, and $N=10$. Figures 7(b) and 7(c) show that an applied input pulse induces changes in γ and ρ. This may be understood from the $2\alpha^2$ terms in Eqs. (54) and (55). The results of the AMM shown by solid curves in Figs. 7(a)–7(c) are in good agreement with DS results shown by dashed curves. Figure 7(d) will be discussed shortly.

It is possible to discuss the synchrony in a neuronal ensemble with the use of γ and ρ defined by Eqs. (46) and (47)

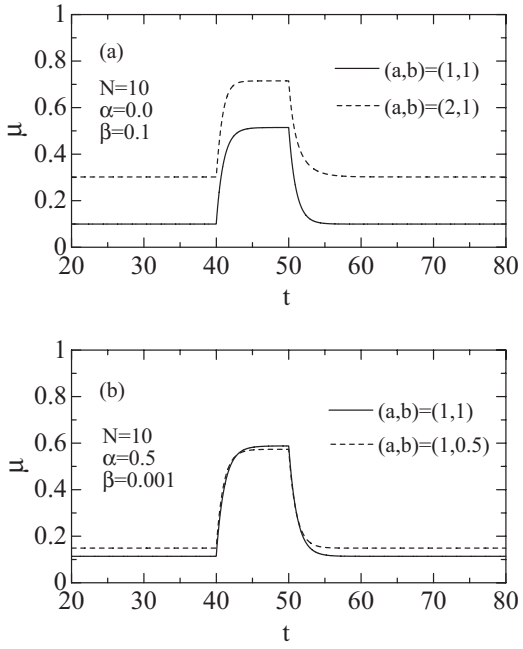

FIG. 8. (a) Response of $\mu(t)$ to input pulse $I(t)$ given by Eq. (59) for $(a,b)=(1,1)$ (solid curve) and $(a,b)=(2,1)$ (dashed curve) with $\alpha=0.0$, $\beta=0.1$, $N=10$, and $\lambda=1.0$. (b) Response of $\mu(t)$ to input pulse $I(t)$ for $(a,b)=(1,1)$ (solid curve) and $(a,b)=(1,0.5)$ (dashed curve) with $\alpha=0.5$, $\beta=0.001$, $N=10$, $\lambda=1.0$, and $w=0.0$.

[18]. In order to quantitatively discuss the synchronization, we first consider the quantity given by

$$P(t)=\frac{1}{N^2}\sum_{ij}\langle[r_i(t)-r_j(t)]^2\rangle=2[\gamma(t)-\rho(t)]. \tag{60}$$

When all neurons are firing with the same rate (the completely synchronous state), we get $r_i(t)=R(t)$ for all i, and then $P(t)=0$ in Eq. (60). On the contrary, we get $P(t)=2(1-1/N)\gamma\equiv P_0(t)$ in the asynchronous state where $\rho=\gamma/N$ [18,41]. We may define the synchronization ratio given by [18]

$$S(t)\equiv 1-\frac{P(t)}{P_0(t)}=\left(\frac{N\rho(t)/\gamma(t)-1}{N-1}\right), \tag{61}$$

which is 0 and 1 for completely asynchronous ($P=P_0$) and synchronous states ($P=0$), respectively. Figure 7(d) shows the synchronization ratio $S(t)$ for $\gamma(t)$ and $\rho(t)$ plotted in Figs. 7(b) and 7(c), respectively, with $\alpha=0.5$, $\beta=1.0$, $w=0.5$, and $N=10$. The synchronization ratio at $t<40$ and $t>60$ is 0.15, but it is decreased to 0.03 at $40<t<50$ by an applied pulse. This is because γ is more increased than ρ by an applied pulse, and the ratio ρ/γ is reduced. The synchronization ratio vanishes for $w=0$, and it is increased with increasing coupling strength [18,41].

Next we show some results for different indices of a and b in $F(x)=-\lambda x^a$ and $G(x)=x^b$. Figure 8(a) shows the time dependence of μ for $(a,b)=(1,1)$ (solid curve) and $(a,b)=(2,1)$ (dashed curve) with $\alpha=0.0$, $\beta=0.1$, $w=0.0$, and $N=10$. The saturated magnitude of μ for $\alpha=0.5$ is larger than that for $\alpha=0.0$. Solid and dashed curves in Fig. 8(b) show μ

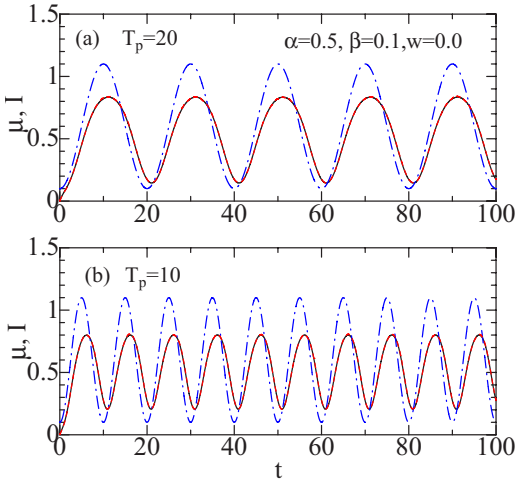

FIG. 9. (Color online) Response of $\mu(t)$ to sinusoidal input $I(t)$ (dot-dashed curves) given by Eq. (62) for $T_p=$(a) 20 and (b) 10 with $A=0.5$, $\lambda=1.0$, $\alpha=0.5$, $\beta=0.1$, $w=0.0$, and $N=10$ ($a=1$ and $b=1$), solid and dashed curves denoting $\mu(t)$ of AMM and dashed curves expressing those of DS result with 100 trials.

for $(a,b)=(1,1)$ and $(1,0.5)$, respectively, with $\alpha=0.5$, $\beta=0.001$, $N=10$, and $w=0.0$. Both results show similar responses to an applied pulse, although μ for a background input of $I^{(b)}=0.1$ for $(a,b)=(1,0.5)$ is a little larger than that for $(a,b)=(1,1)$.

3. Response to sinusoidal inputs

We have applied also a sinusoidal input given by

$$I(t)=A\left[1-\cos\left(\frac{2\pi t}{T_p}\right)\right]+I^{(b)}, \tag{62}$$

for $F(x)=-\lambda x$ and $G(x)=x$ with $\lambda=1.0$, $A=0.5$, $I^{(b)}=0.1$, and $T_p=10$ and 20. Time dependences of μ for $T_p=20$ and $T_p=10$ are plotted in Figs. 9(a) and 9(b), respectively, with $\alpha=0.5$, $\beta=1.0$, $w=0.0$, and $N=10$. AMM results of $\mu(t)$ shown by solid curves in Figs. 9(a) and 9(b) are indistinguishable from DS results (with 100 trials) shown by dashed curves [52], dot-dashed curves denoting the sinusoidal input $I(t)$. As the period of T_p becomes shorter, the magnitude of μ becomes smaller. The delay time of $\mu(t)$ against an input $I(t)$ is about $\tau_d\sim 1.0$ $(=1/\lambda)$ for both $T_p=10$ and $T_p=20$.

III. DISCUSSION

We may calculate variabilities of r and T, by using their distributions of $p(r)$ and $\Pi(T)$, which have been obtained in Sec. II. For example, in the case of $F(x)=-\lambda x$ and $G(x)=x$, the distribution of $p(r)$ for $\beta=0.0$, $w=0.0$, and $H=I$ given by Eq. (26) leads to

$$\langle r\rangle=\frac{I}{(\lambda-\alpha^2/2)}, \tag{63}$$

$$\langle \delta r^2\rangle=\langle(r-\langle r\rangle)^2\rangle=\frac{I^2\alpha^2}{2(\lambda-\alpha^2/2)^2(\lambda-\alpha^2)}, \tag{64}$$

$$\bar{c}_v \equiv \frac{\sqrt{\langle \delta r^2 \rangle}}{\langle r \rangle} = \frac{\alpha}{\sqrt{2(\lambda - \alpha^2)}}. \quad (65)$$

The relevant Γ distribution for ISI, $\Pi(T)$, given by Eq. (33) yields

$$\langle T \rangle = \frac{\lambda}{I}, \quad (66)$$

$$\langle \delta T^2 \rangle = \langle (T - \langle T \rangle)^2 \rangle = \frac{\lambda \alpha^2}{2I^2}, \quad (67)$$

$$c_v \equiv \frac{\sqrt{\langle \delta T^2 \rangle}}{\langle T \rangle} = \frac{\alpha}{\sqrt{2\lambda}}. \quad (68)$$

Equations (65) and (68) show that both $\bar{c}_v$ and c_v are increased with increasing magnitude (α) of multiplicative noise.

It has been reported that spike train variability seems to be correlated with location in the processing hierarchy [53]. A large value of c_v is observed in the hippocampus ($c_v \sim 3$) [54] whereas c_v is small in cortical neurons ($c_v \sim 0.5-1.0$) and motor neurons ($c_v \sim 0.1$) [55,56]. In order to explain the observed large c_v, several hypotheses have been proposed: (1) a balance between excitatory and inhibitory inputs [57,58], (2) correlated fluctuations in recurrent networks [59], (3) active dendrite conductance [60], and (4) a slowly decreasing tail of input ISI of T^{-d} ($d>0$) at large T [61]. Our calculation shows that multiplicative noise may be an alternative origin (or one of the origins) of the observed large variability. We note that the variability of r is given by $\bar{c}_v = \sqrt{\gamma}/\mu$ in the AMM [e.g., Eq. (65) agrees with $\sqrt{\gamma}/\mu$ for μ and γ given by Eqs. (56) and (57), respectively, with $w=\beta=0$]. It would be interesting to make a more detailed study of the variability for general $F(x)$ and $G(x)$ as discussed in Sec. II.

We have proposed the generalized rate-code model given by Eqs. (5) and (6), in which the relaxation process is given by a single $F(x)$. Instead, when the relaxation process consists of two terms

$$F(x) \to c_1 F_1(x) + c_2 F_2(x), \quad (69)$$

with $c_1 + c_2 = 1$, the distribution becomes

$$p(r) = [p_1(r)]^{c_1} [p_2(r)]^{c_2}, \quad (70)$$

where $p_k(r)$ ($k=1,2$) denotes the distribution only with $F(x)=F_1(x)$ or $F(x)=F_1(x)$. In contrast, when multiplicative noise arises from two independent origins,

$$\alpha x \eta(t) \to c_1 \alpha_1 x \eta_1(t) + c_2 \alpha_2 x \eta_2(t), \quad (71)$$

the distribution for $\beta=H=0$ becomes

$$p(r) \propto r^{-[2\lambda/(c_1\alpha_1^2 + c_2\alpha_2^2)+1]}. \quad (72)$$

Similarly, when additive noise arises from two independent origins,

$$\beta \xi(t) \to c_1 \beta_1 \xi_1(t) + c_2 \beta_2 \xi_2(t), \quad (73)$$

the distribution for $\alpha=H=0$ becomes

$$p(r) \propto e^{-\lambda/(c_1\alpha_1^2 + c_2\alpha_2^2)}. \quad (74)$$

Equations (70), (72), and (74) are quite different from the form given by

$$p(r) = c_1 p_1(r) + c_2 p_2(r), \quad (75)$$

which has been conventionally adopted for a fitting the theoretical distribution to that obtained by experiments [36–40].

IV. CONCLUSION

We have proposed a generalized rate-code model [Eqs. (5) and (6)], whose properties have been discussed by using the FPE and the AMM. The proposed rate model is a phenomenological one and has no biological basis. As discussed in Sec. I, the conventional rate model given by Eq. (1) may be obtainable from a spiking neuron model when we adopt appropriate approximations to DEs derived by various approaches such as the population-density method [12–16] and others [19–21]. It would be interesting to derive our rate model given by Eqs. (5) and (6), starting from a spiking neuron model. The proposed generalized rate model is useful in discussing stationary and dynamical properties of neuronal ensembles. Indeed, our rate model has an interesting property, yielding various types of stationary non-Gaussian distributions such as Γ, inverse-Gaussian, and log-normal distributions, which have been experimentally observed [36–40]. It is well known that the Langevin-type model given by Eq. (1) cannot properly describe fast neuronal dynamics at characteristic times τ_c shorter than τ ($\equiv 1/\lambda$). This is, however, not a fatal defect because we may evade it, by adopting an appropriate τ value of $\tau < \tau_c/10$ for a given neuronal ensemble with τ_c. Actually, the dynamical properties of an ensemble consisting of excitatory and inhibitory neurons has been successfully discussed with the use of the Langevin-type Wilson-Cowan model [12,34] (for recent papers using the Wilson-Cowan model, see [62], and related references therein). One of the disadvantages of the AMM is that its applicability is limited to the case of weak noise because it neglects contributions from higher moments.

On the contrary, the AMM has following advantages.

(i) The dynamical properties of an N-unit neuronal ensemble may be easily studied by solving three-dimensional ordinary DEs [Eqs. (48)–(50)], in which the three quantities μ, γ, and ρ have clear physical meanings.

(ii) Analytic expressions for DEs provide us with physical insight without numerical calculations (e.g., the N dependence of ρ follows the central-limit theorem [Eq. (58)]).

(iii) The synchronization of the ensemble may be discussed [Eq. (61)].

As for item (i), note that we have to solve the N-dimensional stochastic Langevin equations in DS, and the $(2N+1)$-dimensional partial DEs in the FPE. Then the AMM calculation is very much faster than DS: for example, for the

calculation shown in Fig. 9(a), the ratio of the computation time of the AMM to that of DS becomes $t_{AMM}/t_{DS} \sim 1/30\,000$ [63]. We hope that the proposed rate model may be adopted for a wide class of study on neuronal ensembles described by the Wilson-Cowan-type model [64].

ACKNOWLEDGMENT

This work is partly supported by a Grant-in-Aid for Scientific Research from the Japanese Ministry of Education, Culture, Sports, Science and Technology.

[1] F. Rieke, D. Warland, R. Steveninck, and W. Bialek, *Spikes—Exploring the Neural Code* (MIT Press, Cambridge, MA, 1996).
[2] W. M. Ursey and R. C. Reid, Annu. Rev. Physiol. **61**, 435 (1999).
[3] R. C. deCharms and A. Zador, Annu. Rev. Neurosci. **23**, 613 (2000).
[4] R. A. Anderson, S. Musallam, and B. Pesaran, Curr. Opin. Neurobiol. **14**, 720 (2004).
[5] J. K. Chapin, K. A. Moxon, R. S. Markowitz, and M. A. L. Nicolelis, Nat. Neurosci. **2**, 664 (1999).
[6] V. B. Mountcasle, J. Neurophysiol. **20**, 408 (1957).
[7] W. Gerstner and W. Kistler, *Spiking Neuron Models* (Cambridge University Press, Cambridge, U.K., 2002).
[8] A. L. Hodgkin and A. F. Huxley, J. Physiol. (London) **117**, 500 (1952).
[9] L. F. Abbott and C. van Vreeswijk, Phys. Rev. E **48**, 1483 (1993).
[10] A. Treves, Network **4**, 259 (1993).
[11] W. Gerstner, Phys. Rev. E **51**, 738 (1995).
[12] H. R. Wilson and J. D. Cowan, Biophys. J. **12**, 1 (1972).
[13] B. W. Knight, Neural Comput. **12**, 473 (2000).
[14] A. Omurtag, B. W. Knight, and L. Sirovich, J. Comput. Neurosci. **8**, 51 (2000).
[15] E. Haskell, D. Q. Nykamp, and D. Tranchina, Network **12**, 141 (2000).
[16] J. Eggert and J. L. van Hemmen, Phys. Rev. E **61**, 1855 (2000).
[17] R. Rodriguez and H. C. Tuckwell, Phys. Rev. E **54**, 5585 (1996).
[18] H. Hasegawa, Phys. Rev. E **67**, 041903 (2003).
[19] D. J. Amit and M. V. Tsodyks, Network **2**, 259 (1991).
[20] B. Ermentrout, Neural Comput. **6**, 679 (1994).
[21] O. Shriki, D. Hansel, and H. Sompolinsky, Neural Comput. **15**, 1809 (2003).
[22] N. Brunel, J. Comput. Neurosci. **8**, 183 (2000).
[23] Z. F. Mainen and T. J. Sejnowski, Science **268**, 1503 (1995).
[24] M. A. Muñoz, in *Advances in Condensed Matter and Statistical Mechanics*, edited by E. Korutcheva and R. Cuerno (Nova Science Publishers, New York, 2004), p. 34.
[25] M. A. Muñoz, F. Colaiori, and C. Castellano, Phys. Rev. E **72**, 056102 (2005).
[26] C. Van den Broeck, J. M. R. Parrondo, and R. Toral, Phys. Rev. Lett. **73**, 3395 (1994).
[27] C. Tsallis, J. Stat. Phys. **52**, 479 (1988).
[28] C. Tsallis, R. S. Mendes, and A. R. Plastino, Physica A **261**, 534 (1998).
[29] G. Wilk and Z. Wlodarczyk, Phys. Rev. Lett. **84**, 2770 (2000).
[30] H. Sakaguchi, J. Phys. Soc. Jpn. **70**, 3247 (2001).
[31] C. Anteneodo and C. Tsallis, J. Math. Phys. **44**, 5194 (2003).
[32] H. Hasegawa, Physica A **365**, 383 (2006).
[33] H. Hasegawa, J. Phys. Soc. Jpn. **75**, 033001 (2006).
[34] S. Amari, IEEE Trans. Syst. Man Cybern. **2**, 643 (1972).
[35] J. J. Hopfield, Proc. Natl. Acad. Sci. U.S.A. **79**, 2554 (1982).
[36] G. L. Gerstein and B. Mandelbrot, Biophys. J. **4**, 41 (1964).
[37] H. C. Tuckwell, *Introduction to Theoretical Neurobiology and Stochastic Theories* (Cambridge University Press, New York, 1988).
[38] D. E. F. McKeegan, Brain Res. **929**, 48 (2002).
[39] R. E. Kass, V. Ventura, and E. N. Brown, Neurophysiology **94**, 8 (2005).
[40] T. P. Vogels, K. Rajan, and L. F. Abbott, Annu. Rev. Neurosci. **28**, 357 (2005).
[41] H. Hasegawa, Physica A **374**, 585 (2007).
[42] H. Hasegawa, Phys. Rev. E **68**, 041909 (2003).
[43] H. Hasegawa, Phys. Rev. E **70**, 021911 (2004).
[44] H. Hasegawa, Phys. Rev. E **70**, 021912 (2004).
[45] H. Hasegawa, Phys. Rev. E **70**, 066107 (2004).
[46] H. Hasegawa, Phys. Rev. E **72**, 056139 (2005).
[47] H. Hasegawa, Phys. Rev. E **61**, 718 (2000).
[48] S. Wang, W. Wang, and F. Liu, Phys. Rev. Lett. **96**, 018103 (2006).
[49] Y. Hayashi, Neural Comput. **6**, 658 (1994).
[50] L. H. A. Monteiro, M. A. Bussab, and J. G. C. Berlinck, J. Theor. Biol. **219**, 83 (2002).
[51] S. Abe and A. K. Rajagopal, J. Phys. A **33**, 8723 (2000).
[52] AMM calculations have been performed by using the second-order Runge-Kutta method with a time step of 0.01. Direct simulations for Eqs. (5) and (6) have been performed by using the Heun method with a time step of 0.0001: DS results are averages of 100 trials unless otherwise noted.
[53] K. D. Harrris, Nat. Rev. Neurosci. **6**, 399 (2005).
[54] A. A. Fenton and R. U. Muller, Proc. Natl. Acad. Sci. U.S.A. **95**, 3182 (1998).
[55] W. R. Softky and C. Koch, Neural Comput. **4**, 643 (1992).
[56] W. Calvin and C. Stevens, J. Neurophysiol. **31**, 574 (1968).
[57] M. Shadlen and W. T. Newsome, Curr. Opin. Neurobiol. **4**, 569 (1994).
[58] T. W. Troyer and K. D. Miller, Neural Comput. **10**, 1047 (1098).
[59] M. Usher, M. Stemmer, C. Koch, and Z. Olami, Neural Comput. **6**, 795 (1994).
[60] W. R. Softky, Curr. Opin. Neurobiol. **5**, 239 (1995).
[61] J. Feng and D. Brown, J. Phys. A **31**, 1239 (1998).
[62] M. Enculescu and M. M. Bestehorn, Phys. Rev. E **67**, 041904 (2003); A. Tonneilier, Physica D **210**, 118 (2005); M. Stetter, Phys. Rev. E **73**, 031903 (2006).
[63] The ratio of the computation time of the AMM to that of DS for the N-unit Langevin model is given by $t_{AMM}/t_{DS} \sim (3/NN_t)(\Delta t_{DS}/\Delta t_{AMM})$, where N_t denotes the trial number of

DS, and Δt_{AMM} and Δt_{DS} are the time steps of the AMM and DS calculations, respectively. For example, this ratio becomes 1/30 000 for the calculation shown in Fig. 9(a), for which $N=10$, $N_t=100$, $\Delta t_{AMM}=0.01$, and $\Delta t_{DS}=0.0001$ [52]; DSs for multiplicative noise require finer time steps than those for additive noise.

[64] H. Hasegawa, in *Neuronal Network Horizons*, edited by M. L. Weiss (Nova Science Publishers, New York, 2007).